Film-Loaded SAW Waveguides for Integrated Acousto-Optical Polarization Converters

Oscar A. Peverini, Harald Herrmann, *Member, IEEE*, and Renato Orta, *Senior Member, IEEE*

***Abstract*—We report on a detailed theoretical and experimental investigation of film-loaded surface acoustic wave (SAW) waveguides in lithium niobate ($LiNbO_3$) for integrated acousto-optical (AO) polarization converters. The numerical analysis is based on both a scalar and a full-vectorial model. Dispersion plots and figures of merit for several structures are given, which lead to design parameters for optimized polarization converters. It is pointed out that very attractive structures are metal/dielectric/$LiNbO_3$ strip waveguides and dielectric/$LiNbO_3$ slot waveguides, in which metal is either gold (Au) or aluminum (Al), and the dielectric film is an optical transparent material such as silicon oxide (SiO_2), magnesium oxide (MgO), or aluminium oxide (Al_2O_3). Polarization converters with the designed acoustical waveguides have been realized and characterized by optical conversion and laser probing measurements.**

I. Introduction

During recent years, a variety of integrated acousto-optical $LiNbO_3$-devices has been developed, mostly for applications in wavelength division multiplexing (WDM) optical communication systems [1]–[3] and sensing applications [4]. The central building block of these devices is the acousto-optical (AO) polarization converter. Due to the interaction of a surface acoustic wave (SAW) with optical waves guided in Ti-indiffused stripe waveguides (fabricated in X-cut, Y-propagating $LiNbO_3$) a wavelength selective polarization conversion (i.e., transverse electric (TE) → transverse magnetic (TM) or TM → TE) is performed.

A propagating SAW induces a periodic perturbation of the dielectric tensor, which results in a coupling of orthogonally polarized optical modes. To achieve an efficient polarization conversion, the process must be phase matched (i.e., the difference between the wave numbers of the optical modes must be compensated by the wave number of the SAW):

$$\left|n_{\text{eff}}^{\text{TE}} - n_{\text{eff}}^{\text{TM}}\right| / \lambda_0 = f_{\text{SAW}} / V_{\text{SAW}}, \tag{1}$$

where f_{SAW} and V_{SAW} are the frequency and the velocity of the SAW, respectively; $n_{\text{eff}}^{\text{TE}}$ and $n_{\text{eff}}^{\text{TM}}$ are the effective indices of the TE and TM polarized optical modes. The phase-matching condition makes the conversion process wavelength selective, so that the optical wavelength λ_0 of the mode to be converted can be adjusted via the radio frequency (RF) applied to the interdigital transducer. For wavelength in the third communication window around $\lambda_0 = 1.55$ μm the RF for phase matching is about 170 MHz, and the tuning slope is about 8 nm/MHz.

Nowadays, most of the AO devices take advantage of integrated acoustical waveguides to confine the SAWs into localized regions, yielding large acoustical power densities even at moderate overall acoustic power levels. The most common technique to fabricate SAW waveguides (SAWG) is via Ti-indiffusion into the cladding regions of the waveguide, which stiffens the material and, hence, increases the acoustic velocity [5]. The SAW is guided in the undoped region between the Ti-indiffused claddings. Such guiding structures are reliable, easy to fabricate, and compatible with the other processing technologies applied for the fabrication of integrated AO devices in $LiNbO_3$. The acoustical waveguides typically induce losses of only 0.5 dB/cm or less for the guided SAW. However, the small SAW velocity change of about 0.3% in the Ti-diffused regions relative to the undoped material requires relatively broad acoustical guides (typically, 100 μm and more) [5]. Furthermore, optical waves may leak into the Ti-diffused boundaries of the acoustical guides if the separation between the optical waveguides and the acoustical boundaries are not large enough. Therefore, the objective of this work was to look for alternative means to fabricate acoustic waveguides with a tighter confinement of the SAWs. This promises also a reduced RF-drive power for the converters and a larger integration density.

It is well-known that, in addition to Ti-indiffusion, other techniques can be applied to realize acoustical waveguides [6]. Recently, AO devices with new film-loaded SAWG have been reported [7], [8], in which the SAW velocity is decreased in the core region by the deposition of an optical transparent material such as SiO_2 [7] or In_2O_3-doped SiO_2 [8]. In the case of a pure SiO_2 film, the confinement of the SAW is almost the same as in the Ti-indiffused SAWG, but the confinement can be remarkably increased by adding the In_2O_3 compound. Although this new type of SAWG appears to be very attractive for integrated AO devices, up to now a detailed numerical and experimental investigation has not been published yet. However, a profound understanding of the SAWG is a prerequisite for the optimization of integrated AO devices. Therefore, in this paper we investigate film-loaded strip and slot waveg-

Manuscript received October 28, 2003; accepted June 14, 2004.
O. A. Peverini and R. Orta are with IEIIT-CNR c/o Politecnico di Torino, Torino, TO, Italy (e-mail: oscar.peverini@polito.it).
H. Hermann is with Universität - GH Paderborn, Angewandte Physik, Paderborn, Germany.

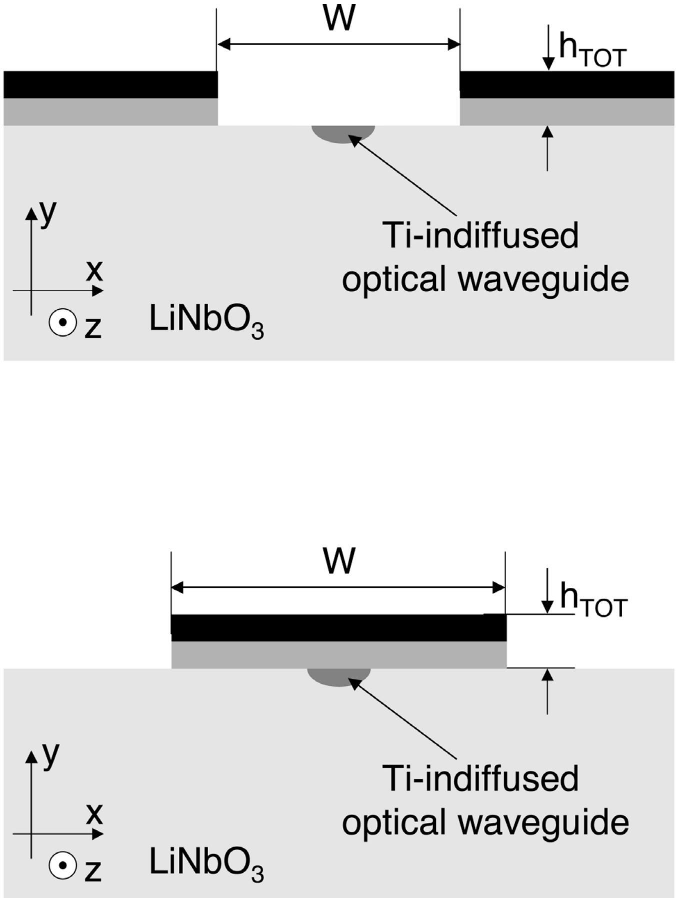

Fig. 1. Stripe-type (lower diagram) and slot-type (upper diagram) film-loaded acoustical waveguides. Black and grey regions refer to metal and dielectric layers, respectively. The total thickness of the layered structure deposited on top of the $LiNbO_3$ substrate is denoted by h_{TOT}.

uiding structures (Fig. 1) for the applicability in integrated AO polarization converters. The numerical analysis of the acoustical waveguides is based both on a scalar model [9] and a full-vectorial model [10]; the modes of the Ti-indiffused optical waveguide are computed via the finite-element method (FEM) [11]. The numerical analysis has been applied to metal/dielectric/$LiNbO_3$ stripe waveguides and to dielectric/$LiNbO_3$ slot waveguides, in which the metal overlay is either Au or Al; and the dielectric film is an optical transparent material such as SiO_2, MgO, or Al_2O_3. Dispersion curves and figures of merit for several structures are reported, from which design parameters for optimized AO polarization converters can be derived.

On the basis of the numerical analysis, some polarization converters with new film-loaded SAW waveguides have been fabricated. The guiding properties of the SAWG have been studied as well as the AO conversion.

II. Numerical Methods for the Analysis of Film-Loaded SAWG

For a preliminary analysis of the film-loaded waveguides a one-dimensional (1-D) model is used, in which only the dominant SAW elongation component is considered [9]. This model provides a simple and computational-efficient method for the investigation and design of film-loaded SAWG. Such a model already has been applied extensively for the design of Ti-diffused acoustical waveguides and directional couplers [12], [13]. But this scalar model does not take into account the anisotropy of materials as well as the influence of the step discontinuities and does not provide the 2-D modal profiles, which are necessary for the evaluation of the AO interaction as reported in Section IV. For these reasons the acoustical waveguides also are analyzed via a full-vectorial model based on the multimode transverse resonance technique (MTRT) [10], in which the waveguiding structure is accurately described by a multimode equivalent network. In both models, a modal analysis in the depth direction of the planar regions composing the waveguides is carried out via a pseudo-spectral elements method (PSEM) [9].

A. Modal Analysis of Planar Piezoelectric Waveguides

Both the scalar and the full-vectorial model require the knowledge of a certain number of modes of each planar stratified region composing the 3-D SAWG. Planar stratified media are typically analyzed along the depth direction via the T-matrix model [14], matrix methods [15], and the impedance model [16]. The propagation constants of guided modes then can be found by imposing the transverse resonance condition and solving the resulting transcendental dispersion equation. Though complex-function theory can be invoked, automated search for the roots, however, is a hard task and some of them may be missed. To overcome this drawback, we adopted the PSEM reported in [9], that allows to compute modal fields and propagation constants without solving any transcendental equation. The basic concept is the expansion of the fields on a set of functions [17]. The differential problem turns into an algebraic generalized eigenvalue one, in which the eigenvalues are the propagation constants, the field configuration are readily obtained as linear combinations of the expansion functions, the weights of which are the eigenvector elements. An exponential convergence is ensured if Legendre polynomials are adopted as expansion functions [18].

B. Scalar Model

A SAW in a piezoelectric material such as $LiNbO_3$ is completely described by four components: the elongations along the three geometrical directions and the electrical potential. For X-cut, Y-propagating SAWs the amplitude of the elongation parallel to the crystalline X-direction (geometrical y-axis in Fig. 1) is dominant [19]. Therefore, we assume that the SAW can be described reasonably well in a scalar approximation by regarding only this component. Similar to the effective index method for optical strip waveguides [20], a reduction to a 1-D problem can be made using a 1-D velocity profile $V_{\mathrm{SAW}}(x)$ in the transverse di-

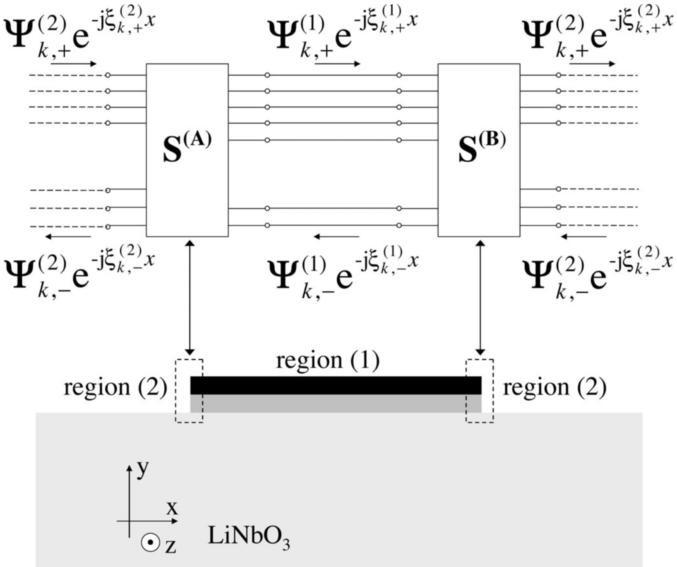

Fig. 2. Transverse equivalent network of film-loaded acoustical waveguides. In the figure $\Psi_{k,+}^{(i)}$ and $\Psi_{k,-}^{(i)}$, with $i = 1, 2$, denote the field profiles in the depth direction of the k-th progressive and of k-th regressive mode in the 2-D planar region, which are identified by propagation constants along the x-direction $\xi_{k,+}^{(i)}$ or $\xi_{k,-}^{(i)}$, respectively.

rection. Once the velocity profile $V_{\mathrm{SAW}}(x)$ has been computed, we need to solve the scalar, 1-D wave equation:

$$\left\{\frac{\partial^2}{\partial x^2} - (2\pi f)^2 \left(\frac{1}{V_{\mathrm{SAW,eff}}^2} - \frac{1}{V_{\mathrm{SAW}}^2(x)}\right)\right\} u_y(x) = 0, \tag{2}$$

where $u_y(x)$ and $V_{\mathrm{SAW,eff}}$ are the transversal field distribution of the elongation along the y-direction and the propagation velocity of the guided SAW mode, respectively. If we further assume that $u_y(x)$ and its first derivative are continuous at the boundaries, we can easily solve this equation and obtain the modes of the structure.

C. Full-Vectorial Model

One extremely useful and accurate technique for obtaining the modes of a waveguide (electromagnetic [21] or acoustic [22]) is the so-called multimode transverse resonance technique, which requires the prior formulation of a transverse equivalent network, representative of the waveguide cross section. In it, an equivalent transmission line direction is chosen to coincide with a direction perpendicular to the actual propagation direction z of the waveguide. As the deposited layers on the top of the substrate are quite thin, a transverse resonance technique along the x-direction of the waveguides under investigation has to be adopted (Fig. 2) [22]. In Fig. 2 $\Psi_{k,+}^{(i)}$ and $\Psi_{k,-}^{(i)}$, with $i = 1, 2$, denote the field profiles in the depth direction of the k-th progressive and of k-th regressive mode in the 2-D planar region (i), which are identified by propagation constants along the x-direction $\xi_{k,+}^{(i)}$ or $\xi_{k,-}^{(i)}$, respectively. For general anisotropic media $\xi_{k,-}^{(i)} \neq -\xi_{k,+}^{(i)}$, a one-directional transmission line has to be associated to each mode. Both the state vector $\Psi_{k,\mp}^{(i)}(y)$ and the propagation constant $\xi_{k,\mp}^{(i)}$ are functions of the angular frequency ω and of the propagation constant along the z-direction β_{AC}. The $\mathbf{S}^{(A)}$ and $\mathbf{S}^{(B)}$ are the generalized scattering matrices (GSM) associated to the steps of the film-loaded waveguide at the sections A and B, respectively.

In order to evaluate the GSM of each single step, the equations describing the relevant boundary and continuity conditions are solved by the mode matching technique (MMT). This is a well established technique in the analysis of discontinuity problems in electromagnetic waveguides and was recently applied to SAW problems [23].

Once the relevant blocks of the transverse equivalent network have been evaluated, the modes of the film-loaded waveguide can be computed by searching for the zeros of the transverse resonance condition [10]:

$$\det\left(\mathbf{I} - \mathbf{S}_{22}^{(A)} \mathrm{e}^{+\jmath\xi_{-}^{(1)}W} \mathbf{S}_{11}^{(B)} \mathrm{e}^{-\jmath\xi_{+}^{(1)}W}\right) = 0. \tag{3}$$

In (3) the following matrix notation has been adopted:

$$\mathbf{S} = \begin{bmatrix} \mathbf{S}_{11} & \mathbf{S}_{12} \\ \mathbf{S}_{21} & \mathbf{S}_{22} \end{bmatrix}, \tag{4}$$

and, hence, $\mathbf{S}_{22}^{(A)}$ and $\mathbf{S}_{11}^{(B)}$ are the left and right reflection blocks of $\mathbf{S}^{(A)}$ and $\mathbf{S}^{(B)}$, respectively. In applying the transverse resonance condition, it is very convenient to subdivide the modes in region (1) into accessible and localized modes. Only the first class is considered in the resonance condition. In fact, the second class consists of the cut-off modes that are so strongly attenuated they do not interact appreciably with the neighboring step. This implies an efficient code because the matrix, whose determinant has to be evaluated, has a size equal to the number of accessible modes.

III. Acoustical Waveguides for AO Devices

Two different types of film-loaded acoustical waveguides for integrated AO polarization converters in $LiNbO_3$ have been investigated: stripe and slot-type waveguides (Fig. 1). The first type consists of a layer or a layer system deposited in the core region of the acoustical guide. This means, to achieve guiding the SAW velocity in the film-loaded region must be smaller than the velocity of the unloaded substrate. For AO polarization converters, one has to consider that the film is on top of the optical waveguide as well. Therefore, the film should not strongly influence the properties of the optical waveguide; especially, no significant loss should be induced for the optical waves. In slot-type guides, the cladding regions of the acoustical guide are covered with a film. Therefore, the film-loading must result in an increase of the SAW velocity to obtain guiding.

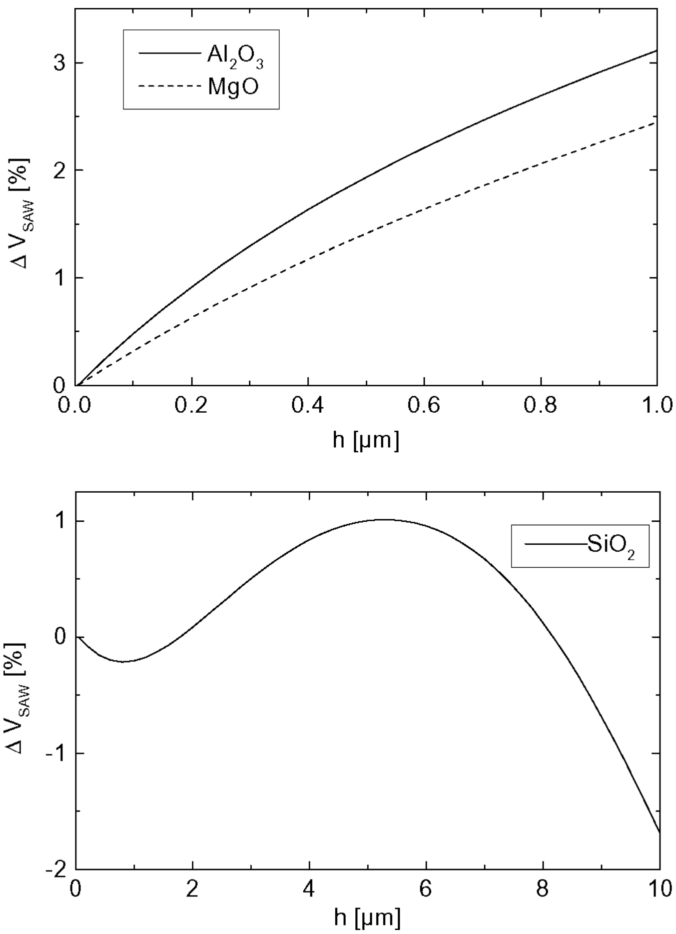

Fig. 3. Calculated SAW velocity change in a dielectric/X–Y $LiNbO_3$ planar structure as a function of the dielectric overlay thickness h at $f = 170$ MHz. Lower diagram: SiO_2. Upper diagram: MgO and Al_2O_3 film, respectively.

A. Acoustical Planar Structures

To study the influence of deposited films on top of $LiNbO_3$ substrate, the SAW velocity change has been calculated. In the simulations, we used the material constants reported in [24] for Al, Au, MgO, and SiO_2, in [25] for $LiNbO_3$, and in [26] for Al_2O_3. In Fig. 3 the calculated relative velocity changes ΔV are shown for a substrate loaded with different materials as a function of the film thickness. The relative velocity changes refer to SAW velocity in X-cut Y-propagating $LiNbO_3$ ($V = 3697$ m/s). The frequency is set to 170 MHz. The lower diagram has been calculated assuming a SiO_2 film. The velocity change varies as function of the film thickness. For a thin layer (i.e., $h < 2$ μm), the change is negative; but for layer thickness between about 2 μm and 8 μm the velocity change is positive. For thicker films, the velocity approaches the SAW velocity of bulk SiO_2, which is smaller than the velocity of $LiNbO_3$. The maximum velocity reduction for small layer thickness is about 0.3%, which is comparable to the velocity change of Ti-diffused guides. Therefore, it should be possible to realize stripe waveguides with simple SiO_2 films, but it cannot be expected to get a better confinement of the SAW mode as for Ti-diffused guides. Moreover, the strong velocity reduction for thick layers seems to be less appropriate for integrated AO devices as a processing of very thick layers would be necessary.

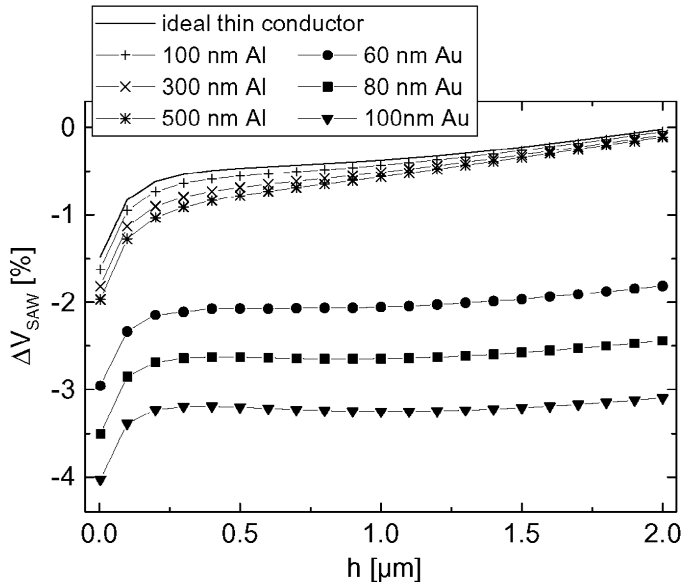

Fig. 4. Calculated SAW velocity change induced by a layer system consisting of SiO_2 as a buffer layer and a metal versus the buffer layer thickness. The frequency is set to 170 MHz. Results for various thicknesses of the Al or Au metal layer are shown. Additionally, the solid curve represents the velocity change induced by an ideal thin conductor on top of the buffer layer.

Other possible materials for deposition on the surface of $LiNbO_3$ are MgO and Al_2O_3. The corresponding calculated SAW velocity changes as a function of the layer thickness are shown in the upper diagram of Fig. 3. These structures consist of a fast film on top of a slow substrate, so that the range of existence of a nonleaky Rayleigh wave is limited to values beyond the cutoff thresholds. One observes a monotonically increase of SAW velocity in the range of existence. For layer thicknesses of about 0.5 μm the velocity change is already more than 2%. Therefore, it should be possible to realize slot-type acoustical waveguides with a good confinement of the SAW.

Instead of using a single SiO_2 film, a layer system might be used as well. It is well known that a metal layer on top of the substrate slows down the SAW velocity. This is due to the short circuiting of the surface as well as to the mass loading. As depositing a metal layer directly on the substrate would induce strong losses for the optical waves, a dielectric buffer layer is required. Therefore, we studied the SAW velocities of $LiNbO_3$ covered with a layer system consisting of a dielectric layer followed by a metal layer. The thickness of the buffer layer should be large enough to avoid additional optical losses.

In Fig. 4 the SAW velocity change at 170 MHz is plotted as a function of the thickness of the SiO_2 layer, which is used as a buffer layer. The metal layer consists of either aluminium or gold. As expected, with such layer systems the SAW velocity is slowed down. The solid line shown in

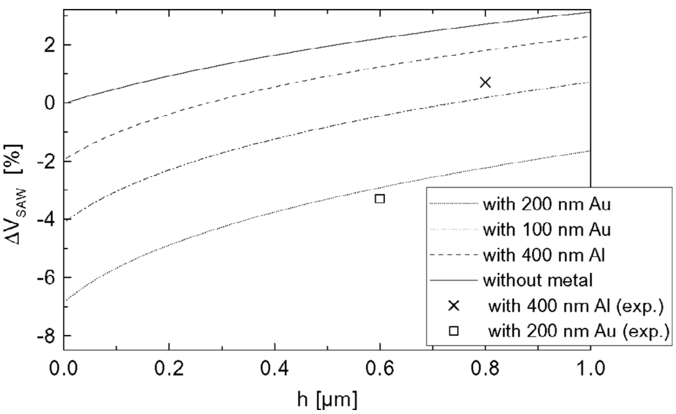

Fig. 5. Calculated SAW velocity change induced by a layer system consisting of Al_2O_3 and 400-nm thick Al-film, 100-nm thick Au-film, or 200-nm thick Au-film, respectively, as a function of the Al_2O_3 layer thickness. The frequency is set to 170 MHz. For comparison, the velocity change induced by pure layer Al_2O_3 is plotted as well. Additionally, some experimental data also are given in the diagram.

the diagram refers to an infinitesimal thin ideal conductor on top of the buffer layer. This means, this conductor induces a short circuiting but no mass loading. It becomes clear from the results that the short circuiting leads to a decrease of the SAW velocity of about 0.5% for a buffer layer thickness of 0.5 μm. The additional decrease of the SAW velocity is due to the mass-loading. Therefore, using Al as metal results in a relatively small change of the SAW velocity; but Au (high density metal) induces velocity changes in the order of a few percent already with very thin layers.

From these numerical results Au/SiO_2 stripe waveguides appear to be very attractive for AO devices because of a large change of the SAW velocity in the core region of the waveguides. Unfortunately, experimental investigation of the acoustical properties of planar SiO_2 films obtained by e-beam evaporation revealed that these structures exhibit acoustical losses in the range of $6 \div 10$ dB/cm, depending on the width of the waveguide. It is known that the acoustical properties of SiO_2 are strongly dependent on the fabrication processes. For instance, films with low acoustic losses can be fabricated using RF magnetron sputtering [27] or plasma enhanced chemical vapor deposition (PECVD) [28]. However, these techniques were not available in our laboratory. Therefore, we concentrated on the investigation of strip waveguides with an Al_2O_3 film as a buffer layer.

As discussed above using Al_2O_3 as dielectric material, the SAW velocity increases. Nevertheless, with an additional metal on top of the dielectric film, the SAW velocity can be remarkably decreased as the SAW velocity increase due to the dielectric overlay is overcompensated by the mass-loading effect of the metal film. Some numerical results are shown in Fig. 5. The relative SAW velocity change at 170 MHz is plotted versus the dielectric layer thickness for structures with 400-nm thick Al and 200-nm and 100-nm Au. Furthermore, some experimental data also are reported. They have been obtained by investigating the conversion characteristics of integrated AO polarization converters. These were realized using conventional Ti-indiffused acoustical waveguides. The layer system was deposited on top of a part of the converter. We compared the phase-match frequency for the polarization conversion in the uncoated and in the coated regions. From the frequency shift, the difference of the SAW velocities has been calculated using (1). The frequency shift can be almost completely attributed to the SAW velocity change as the film loading has negligible influence on the effective indices of the optical modes. Moreover, the velocity dispersion due to the guiding effect in the Ti-diffused waveguide could be neglected, too, because of the small change of the SAW velocity relative to the substrate. For small dielectric layer thickness, the mass-loading effect of the metal is dominant. With the Al loading, a negative velocity change is obtained for the Al_2O_3 layer thickness below 0.3 μm. Using the Au film, the effect is much more pronounced. The much higher density of Au results in strong mass loading, and, hence, in a tremendous reduction of the SAW velocity. Even for the Al_2O_3 layer thickness of 0.5 μm, the SAW velocity change is still larger than 3% as also experimentally observed. Moreover, we observed acoustical losses in the range of $2 \div 3$ dB/cm that makes Au/Al_2O_3 stripe waveguides feasible for integrated polarization converters, even if the fabrication parameters could be further optimized in order to achieve losses comparable with those exhibited by Ti-diffused waveguides.

B. Film-Loaded SAW Waveguides for Acousto-Optical Polarization Converters

In Fig. 6 the calculated normalized velocity of the fundamental and of the first three higher order modes of a Au/Al_2O_3 stripe-type waveguide is shown as function of the waveguide width (i.e., the width of the stripe). The Au and Al_2O_3 films are 200-nm and 600-nm thick, respectively; and the SAW frequency has been taken to be 170 MHz. Both the results obtained via the scalar model and via the full-wave model are shown. In Fig. 6, V_{co} and V_{cl} represent the SAW velocity in the core and in the cladding regions of the stripe waveguide, respectively. Because of the anisotropy of the $LiNbO_3$ crystal, the values of these velocities differ slightly in the scalar and in the full-wave models. From these results, one can infer that below about 40-μm width, the acoustical waveguide is single mode; but at larger widths, higher order modes are guided, too. For a 35-μm wide waveguide, the elastic displacements and the electrical potential at a frequency of 170 MHz are displayed in Fig. 7. The fields are normalized so that the SAW power is 10 mW. As in the X–Y $LiNbO_3$ substrate, the SAW still is polarized mainly in the sagital plane (geometrical yz plane), with u_y being the main component. Moreover, due to the strong mass loading induced by the Au film, the lateral confinement of the mode is very pronounced.

On the basis of the numerical results, polarization converters with Au/Al_2O_3 stripe waveguides have been real-

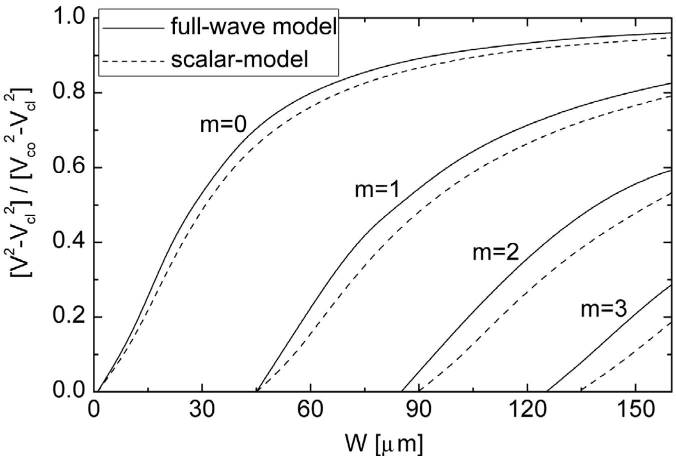

Fig. 6. Calculated normalized modal velocities of the fundamental mode ($m = 0$) and of higher order modes ($m > 0$) in a film-loaded stripe waveguide as a function of the stripe width W at $f_{\mathrm{SAW}} =$ 170 MHz. The data have been calculated assuming a layer system consisting of an Al_2O_3 buffer layer (thickness 600 nm) and an Au-layer of 200-nm thickness. The computations have been performed via both the scalar model and the full-wave model.

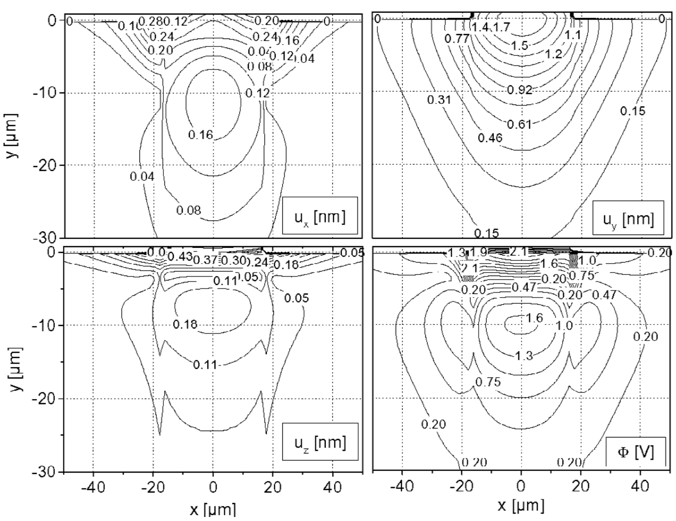

Fig. 7. Calculated fundamental mode of a film-loaded stripe-type acoustical waveguide realized with an Au/Al_2O_3 layer system. The width of the waveguide is 35 μm, the Au-film is 200-nm thick, and the Al_2O_3-layer thickness is 600 nm. For the calculation, a SAW frequency of 170 MHz has been assumed, and the amplitudes have been scaled to guide an acoustical power of 10 mW.

ized. In Fig. 8 the measured conversion characteristics obtained in polarization converters with a 60-μm and 120-μm wide Au/Al_2O_3 acoustical stripe, respectively, are shown. The length of the acoustical waveguides is 60 mm, and the optical waveguides have been fabricated by an indiffusion of 7-μm wide, 100-nm thick Ti stripes. The diffusion has been performed at $T_D = 1060°$C for 9 hours. The optical wavelength is 1552 nm. The conversion characteristics were measured using fixed optical wavelengths and varying the acoustical frequency. This technique is equivalent to fix the acoustical frequency and span the optical wavelength. External polarizers have been used to polarize the

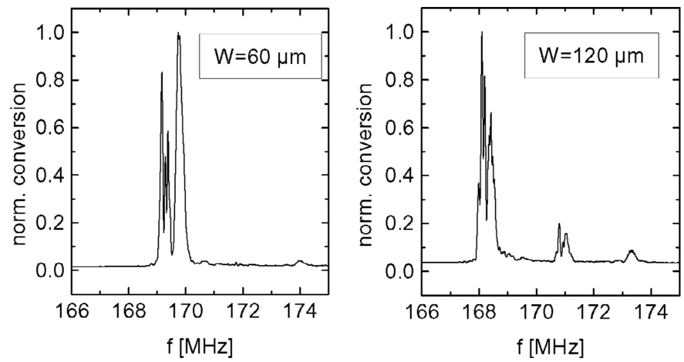

Fig. 8. Measured normalized conversion characteristics obtained with a 120-μm and a 60-μm wide acoustical stripe waveguide, respectively. The waveguide stripe is realized with 200 nm Au on top of a 600-nm thick Al_2O_3-layer. The optical wavelength is 1552 nm.

input optical signal and to select the output polarization. In Fig. 8, the converted power for the two structures is normalized to the corresponding maximum at 169.8 MHz and 168.1 MHz.

For the wider guide, three conversion peaks at different frequencies are observed. They correspond to AO interactions of the optical modes with different acoustical modes. The 120-μm guide is not single mode. From the theoretical analysis (Fig. 6), three acoustical modes can be guided in the structure. This is in reasonably good agreement with the experimentally observed results. The conversion characteristics of the narrower guide shows only one pronounced conversion peak at about 170 MHz and a very small peak at about 174 MHz. The modeling for this guide predicts two guided modes with one being close to cut-off. The structure of the conversion curve is still far away from the theoretically predicted sinc^2-shape. This has to be attributed to inhomogeneites within the structure. The influence of such inhomogeneites become very pronounced as the overall structure with 60 mm extremely is long. Indeed, rejections of only -3 dB and -9 dB to the incident polarization were achieved in the 60-μm and 120-μm wide structures, respectively.

Laser probing measurements [29] have been performed on these structures as well. This technique is based on the measurements of the 0th and 1st order beams diffracted by the surface deformation grating induced by the traveling SAW, when the sample is illuminated. Because the level of the first order diffracted beam is very weak, a lock-in amplifier has to be used to drop the noise level.

Fig. 9 shows the normalized SAW power density measured at $f_{\mathrm{SAW}} = 170$ MHz for the 120-μm wide waveguide. The inset shows the profile of the SAW power along the propagation direction, from which acoustical losses of about 2.5 dB/cm can be inferred.

In the previous section, it was pointed out both theoretically and experimentally that an Al_2O_3 film deposited on top of $LiNbO_3$ increases the SAW velocity. This effect can be exploited in the fabrication of slot-type acoustical waveguides by covering the cladding regions of the $LiNbO_3$ substrate with an Al_2O_3 layer. The main advan-

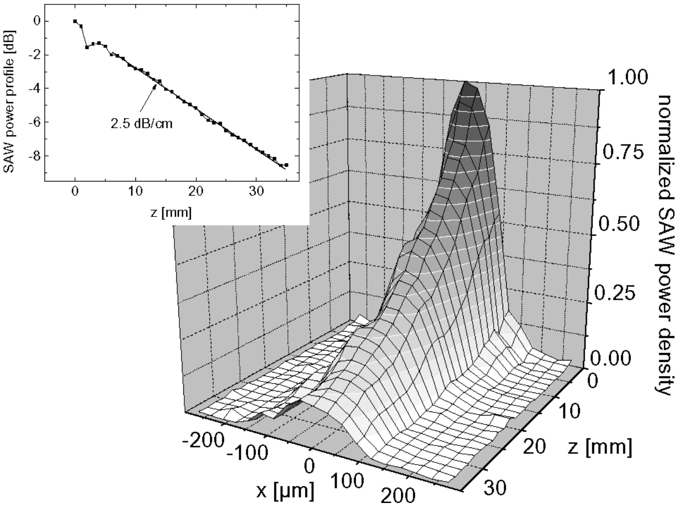

Fig. 9. Result of a laser-probing measurement of the SAW power density in an Au/Al_2O_3-stripe waveguide at $f_{SAW} = 170$ MHz. The Au-film is 200-nm thick and the Al_2O_3-layer thickness is 600 nm. The inset shows the derived SAW power profile along the propagation direction.

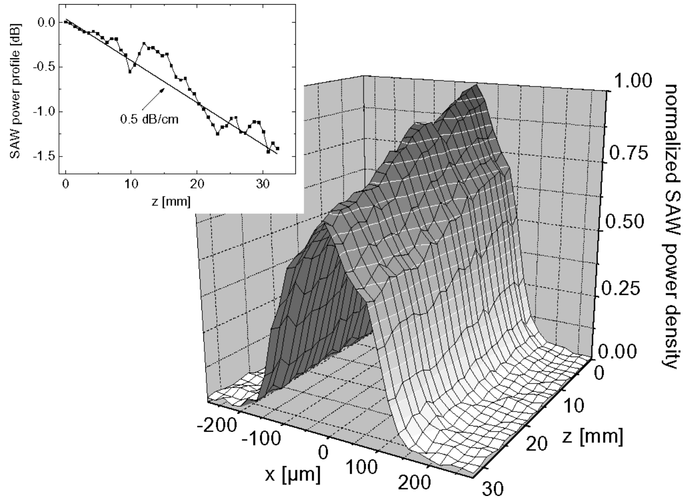

Fig. 11. Result of a laser-probing measurement of the SAW power density in a 100-μm wide Al_2O_3-slot waveguide at $f_{SAW} = 170$ MHz. The Al_2O_3-layer thickness is 800 nm. The inset shows the derived SAW power profile along the propagation direction.

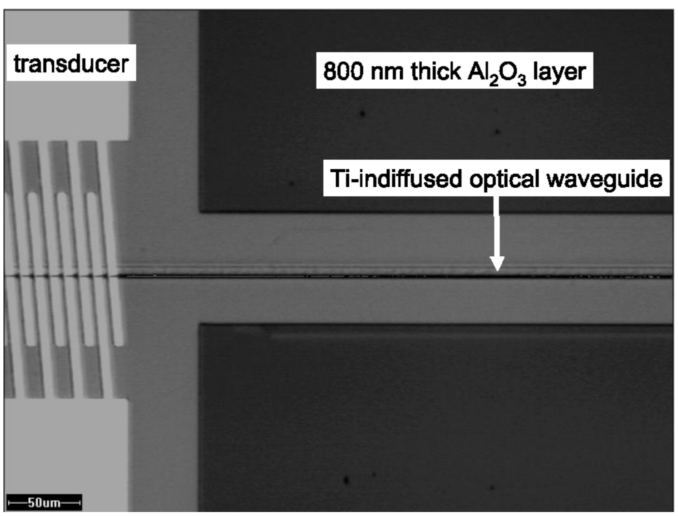

Fig. 10. Micrograph of a fabricated straight AO polarization converter realized with an Al_2O_3-loaded slot waveguide.

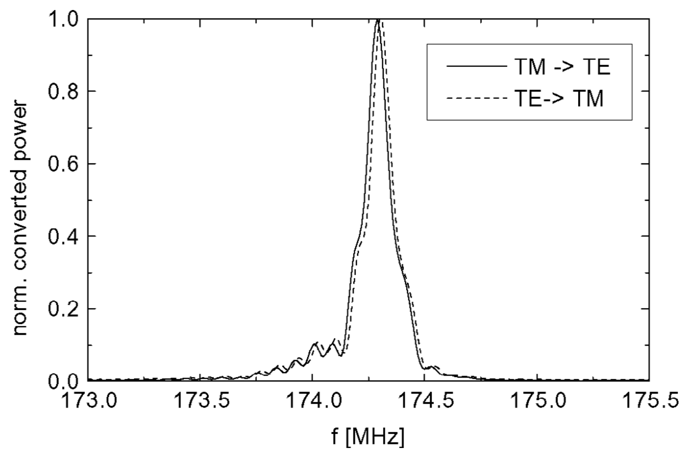

Fig. 12. Measured normalized converted power in a polarization converter realized with an Al_2O_3-slot waveguide. The width of the waveguide is 100 μm, and the Al_2O_3-layer thickness is 800 nm.

tage of these structures in comparison with stripe-type waveguides is that smaller losses have to be expected. In fact, in both configurations the loss mechanism is due to the propagation of the acoustical wave in the overlay. However, in stripe-type structures, the overlay is deposited in the region in which the SAW exhibits its maximum values; and in slot-type waveguides, the losses of the layer affect only the evanescent fields of the SAW. The experimental investigation, slot-type waveguides with an 800-nm thick Al_2O_3 layer and width $W = 40 \div 100$ μm were fabricated (Fig. 10). As expected, all the structures exhibit losses smaller than 1 dB/cm, as can be observed in Fig. 11, in which the result of a laser probing measurement on a 100-μm wide, slot-waveguide is reported. The measured propagation losses in this structure are ≈ 0.5 dB/cm. In Fig. 12 the converted power in the corresponding polarization converter is shown. The converted power is normalized to its maximum at 174.3 MHz, in which a rejection of already ≈ -12 dB to the incident polarization is achieved. The length of the interaction region was set to ≈ 45 mm in order to provide a better homogeneity within the structure and the RF driving power was about 3 dBm. In this case, only a pronounced conversion peak at ≈ 174.3 MHz can be observed; but we could not observe in the conversion characteristics more conversion peaks corresponding to the interaction of the optical modes with higher-order acoustical modes. In fact, in 800-nm thick Al_2O_3-loaded regions, a relative change of the SAW velocity of $\approx -0.7\%$ was measured. Although a higher velocity change was predicted on the basis of the available physical data for Al_2O_3, the SAW velocity can be further decreased by depositing thicker Al_2O_3 films, depending on the technological capabilities. In this converter, lower side lobe values compared to that of the converters with stripe guides are achieved and the structure of the conversion curve is reasonably close to the theoretically predicted sinc^2-shape.

As far as the optical losses are concerned, in Al_2O_3-slot SAWG the film is not deposited on top of the optical waveguides, as in Ti-indiffused SAWG, and, hence, no additional optical losses are to be expected. Moreover, the Al_2O_3 layer is optically transparent, and we have experimentally verified that it does not affect the properties of the optical waveguides in terms of effective modal indices and losses.

IV. Evaluation of the Acousto-Optical Interaction

One important figure of merit for AO devices is the coupling coefficient between the fundamental TE and TM optical modes due to the interaction with the guided SAW [30]:

$$k = \frac{\omega}{8P_0} \iint \mathbf{E}^*_{\mathrm{TM}} \Delta\epsilon \mathbf{E}_{\mathrm{TE}} \mathrm{d}x\mathrm{d}y, \tag{5}$$

where $\mathbf{E}_{\mathrm{TE}}$ and $\mathbf{E}_{\mathrm{TM}}$ are the electrical fields of the fundamental TE and TM optical modes, respectively; P_0 is the power associated to the optical modes; $\Delta\epsilon$ is the modulation of the electrical permeability tensor of $LiNbO_3$ induced by the travelling SAW via the elasto-optic and electro-optic effects:

$$\Delta\epsilon_{ij} = -\frac{1}{\epsilon_0}\epsilon_{ik}\Delta B_{kl}\epsilon_{lj}, \tag{6}$$

where:

$$\Delta B_{ij} = p_{ijkl}S_{kl} + r_{kij}E_k, \tag{7}$$

is the dielectrical impermeability tensor; S_{kl} and E_k are the strain and the electrical field associated to the SAW, $\{p_{ijkl}\}$ and $\{r_{kij}\}$ are the elasto-optical and electro-optical coefficients tensors, respectively.

In the computation of the coupling coefficient in X-cut Y-propagating $LiNbO_3$ devices, the following approximation proves to be very accurate [30]:

$$k \approx k_{yx} = \frac{\omega}{8P_0} \iint \left(E_y^{\mathrm{TM}}\right)^* \Delta\epsilon_{yx} E_x^{\mathrm{TE}} \mathrm{d}x\mathrm{d}y. \tag{8}$$

In order to achieve a high interaction efficiency (i.e., a high coupling coefficient), the overlap integral between the profiles of the optical modes and of the SAW should be maximized. This requires the knowledge of the 2-D profiles of both the optical modes in the Ti-indiffused waveguide and of the modes of the film-loaded acoustical waveguide. The optical modes have been computed via the finite-elements method described in [11]; and the film-loaded acoustical waveguides have been analyzed via the MTRT. In Fig. 13 we plotted the computed coupling coefficient as a function of the waveguide width W for both metal/Al_2O_3 film-loaded stripe waveguides and Al_2O_3 film-loaded, slot waveguides. For the stripe-type structure, the buffer layer thickness is 600 nm in order to provide enough insulation of the optical waveguide from the 200-nm thick Au film; and for the slot configuration, the thickness of the Al_2O_3 layer is 800 nm. The optical waveguides are 7-μm wide, Ti-indiffused waveguides, and the optical wavelength is 1550 nm. One can observe that the stripe-type structure leads to higher coupling coefficients in comparison with the slot waveguide. Indeed, in the stripe configuration the SAW profile in the depth direction is modified in the core region, leading to a better overlap between the acoustical mode and the optical modes. For both structures the maximum coupling coefficients are obtained for waveguide widths at about 40 μm as better overlaps in the lateral direction are achieved. In particular, for the Au/Al_2O_3 structure with 200-nm Au, a coupling coefficient of about 352 m^{-1} can be achieved with a stripe width of 35 μm. This value of the coupling coefficient is about twice that of a 120-μm wide, Ti-diffused waveguide [30], so that the RF driving power necessary for the conversion is reduced by a factor of four.

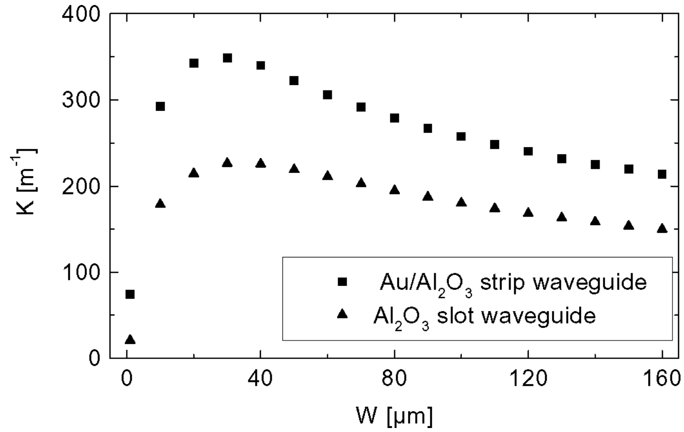

Fig. 13. Calculated coupling coefficient for polarizers converters with stripe and slot acoustical waveguides, respectively, as a function of the waveguide width W. The stripe waveguide is realized with 200 nm Au on top of a 600-nm thick Al_2O_3-layer. In the slot configuration, an 800-nm thick Al_2O_3-film is deposited on the cladding regions. The optical waveguides are 7-μm wide Ti-indiffused waveguides, and the optical wavelength is 1550 nm. For the calculation, a SAW frequency of 170 MHz has been assumed and the acoustical amplitudes have been scaled to guide an acoustical power of 10 mW.

In order to compare the efficiency of AO polarization converters with different straight acoustical waveguides, in Table I the driving power and the interaction length are reported for the structures with Ti-indiffused SAWG [31], [32] and with the presented Al_2O_3-slot SAWG. The comparison is not applicable for the Au/Al_2O_3-stripe waveguides as several acoustical modes are excited in the structure with unknown amplitude ratio. As is well-known, the AO conversion efficiency at perfect phase-matching conditions is given by:

$$\eta = \sin^2\left(\gamma\sqrt{P_{\mathrm{RF}}}L\right), \tag{9}$$

TABLE I
Comparison of the Efficiency of AO Polarization Converters with Different Straight Acoustical Waveguides.

AO polarization converter	RF driving power P_{RF} [mW]	Interaction length L [mm]	Normalized power factor ρ [mW mm^2]
Ti-indiffused SAWG [31]	35	11	4235
Ti-indiffused SAWG [32]	8	30	7200
Al_2O_3-slot SAWG	2	45	4050

with P_{RF} being the driving power, L is the interaction length, and γ is a constant depending on the structure and materials of the AO polarization converter. The complete conversion is achieved when the argument in (9) is equal to $\pi/2$ corresponding to a RF power $P_{\mathrm{RF}} = P_{100\%}$. In order to compare the values of driving power and of interaction length reported in Table I, it is convenient to define a normalized power factor ρ in [mW mm^2] according to:

$$P_{100\%} = \rho/L^2. \tag{10}$$

The smaller the value of the normalized power ρ is, the more efficient is the AO process. The strong difference of ρ for AO polarization converters with Ti-indiffused SAWG calculated from the data present in [31] and [32] is probably due to different coupling conditions of the SAW into the waveguide. An optimization of the finger overlap of the transducer and of its tilt angle allows a more efficient coupling.

From the data reported in Table I, it can be inferred that the presented Al_2O_3-slot SAWGs are comparable in performance with the Ti-indiffused waveguides. However, an optimization of the fabrication process is still possible, which should lead to higher performance AO polarization converters.

V. Conclusions

In this paper we performed numerical and experimental investigations of film-loaded acoustical waveguides for AO polarization converters. The numerical analysis is based on both a scalar model and a full-wave model. From the numerical results, polarization converters with Au/Al_2O_3 and Au/SiO_2 stripe waveguides appear to be very promising structures for integrated AO $LiNbO_3$-devices, as high coupling coefficients and strong acoustical field confinement could be achieved.

Experimental investigation about polarization converters fabricated with Au/Al_2O_3 stripe waveguides confirmed the numerical predictions. However, the fabrication process has to be optimized because these structures exhibit acoustical losses in the range $2\div3$ dB/cm, and optical conversion characteristics are still far away from the predicted ones.

Polarization converters with slot waveguides loaded with a 800-nm thick Al_2O_3 layer have been realized as well. Acoustical losses smaller than 1 dB/cm were measured, and a clear guiding effect was obtained also in a 40-μm wide structure. Optical conversion characteristics are already quite close to the ideal case. Hence, Al_2O_3-based, slot-acoustical waveguides should enable one to increase the integration density of complex AO devices. In fact, the leakage of optical waves in the claddings, as in Ti-diffused waveguides, could be overcome due to the optical transparency of Al_2O_3. Moreover, an optimization of the fabrication process could yield higher SAW velocity changes. This means that even a stronger field confinement is feasible leading to lower drive RF power requirements.

Acknowledgments

The authors would like to thank Prof. Dr. W. Sohler for many valuable discussions and Dipl. Phys.-Ing. R. Ricken for the sample fabrication.

References

[1] D. A. Smith, R. S. Charkravarthy, Z. Bao, J. E. Baran, J. L. Jackel, A. d'Alessandro, D. J. Fritz, S. H. Huang, X. Y. Zou, S. M. Hwang, A. E. Willner, and K. D. Li, "Evolution of the acoustooptic wavelength routing switch," *J. Ligthwave Technol.*, vol. 14, pp. 1005–1019, 1996.

[2] M. K. Smith, A. M. J. Koonen, H. Herrmann, and W. Sohler, "Wavelength-selective device," in *Fiber Optic Communication Devices.* N. Grote and H. Venghaus, Eds. Berlin: Springer-Verlag, 2001, pp. 262–312.

[3] Y. Miyazaki and N. Goto, "Tunable matrix switches and routers consisting of waveguide-type acousto-optic separators with SAW for WDM systems," in *Proc. IEEE Ultrason. Symp.*, 2002, pp. 605–608.

[4] C. Boulet, D. J. Webb, M. Douay, and P. Niay, "Simultaneous interrogation of fiber Bragg grating sensors using an acoustooptic tunable filter," *IEEE Photonic Tech. Lett.*, vol. 13, pp. 1215–1217, Nov. 2001.

[5] H. Herrmann, U. Rust, and K. Schäfer, "Tapered acoustical directional couplers for integrated acousto-optical mode converters with weighted coupling," *J. Ligthwave Technol.*, vol. 13, pp. 364–374, Mar. 1995.

[6] A. A. Oliner, *Acoustic Surface Waves.* Berlin: Springer-Verlag, 1978.

[7] H. Mendis, A. Mitchell, I. Belsky, M. Austin, and O. A. Peverini, "Design, realisation and analysis of an apodized, film-loaded acousto-optic tunable filter," *Appl. Phys. B*, vol. 73, pp. 489–493, 2001.

[8] T. Nakazawa, S. Taniguchi, and M. Seino, "Ti:$LiNbO_3$ acousto-optic tunable filter (AOTF)," *Fujitsu Sci. Tech. J.*, vol. 35, pp. 107–112, July 1999.

[9] O. A. Peverini, R. Orta, and R. Tascone, "Analysis of piezoelectric strip waveguides based on the effective index and pseudospectral element methods," *J. Acoust. Soc. Amer.*, vol. 112, pp. 2623–2633, Dec. 2002.

[10] O. A. Peverini, "SAW waveguides and transducers for acousto-optical devices," Ph.D. dissertation, Politecnico di Torino, Turin, Italy, 2001.

[11] E. Strake, G. P. Bava, and I. Montrosset, "Guided modes of Ti:$LiNbO_3$ channel waveguides: A novel quasianalytical technique in comparison with the scalar finite-element method," *J. Ligthwave Technol.*, vol. 6, pp. 1126–1135, June 1988.

[12] K. Saitoh and M. Koshiba, "Unified software for the design of acoustooptic devices," *IEEE Trans. Magn.*, vol. 36, pp. 1779–1783, July 2000.

[13] A. Bove, G. Donato, S. Schmid, E. DeAmbrogi, I. Montrosset, and G. Perrone, "BPM simulations of surface acoustic waves in

planar waveguide structures on $LiNbO_3$," in *Proc. Eur. Conf. Integrated Opt.*, Turin, Italy, 1999, pp. 51–54.

[14] C. Potel and J. de Belleval, "Propagation in an anisotropic periodically multilayered medium," *J. Acoust. Soc. Amer.*, vol. 93, pp. 2669–2677, May 1993.

[15] E. L. Adler, J. K. Slaboszewicz, G. W. Farnell, and C. K. Jen, "PC software for SAW propagation in anisotropic multilayers," *IEEE Trans. Ultrason., Ferroelect., Freq. Contr.*, vol. 37, pp. 215–223, May 1990.

[16] S. V. Biryukov, Y. V. Gulyaev, V. V. Krylov, and V. P. Plessky, *Surface Acoustic Waves in Inhomogeneous Media.* Berlin: Springer-Verlag, 1995.

[17] Y. Kim and W. D. Hunt, "Acoustic fields and velocities for surface-acoustic-wave propagation in multilayered structures: an extension of the Laguerre polynomial approach," *J. Appl. Phys.*, vol. 68, pp. 4993–4997, Nov. 1990.

[18] V. Lancellotti and R. Orta, "Guided waves in layered cubic media: Convergence study of a polynomial expansion approach," *J. Acoust. Soc. Amer.*, vol. 104, pp. 2638–2644, Nov. 1998.

[19] A. J. Slobodnik, E. D. Conway, and R. T. Delmonico, "Surface wave velocities," *Microwave Acoustics Handbook*, vol. 1A, Cambridge, MA: Air Force Cambridge Research Labs, 1973.

[20] G. B. Hocker and W. K. Burns, "Mode dispersion in diffused channel waveguides by the effective index method," *Appl. Opt.*, vol. 16, pp. 113–118, 1977.

[21] T. Itoh, *Numerical Techniques for Microwave and Millimeter-Wave Passive Structures.* New York: Wiley, 1989.

[22] R. C. M. Li, A. A. Oliner, and H. L. Bertoni, "Microwave network analyses of surface acoustic waveguides—I. Flat overlay guides," *IEEE Trans. Sonics Ultrason.*, vol. SU-22, pp. 66–78, Mar. 1977.

[23] M. Pereira da Cunha and E. L. Adler, "Scattering of SAW at discontinuities: Some numerical experiments," *IEEE Trans. Ultrason., Ferroelect., Freq. Contr.*, vol. 42, pp. 168–173, Mar. 1995.

[24] B. A. Auld, *Acoustic Fields and Waves in Solids.* vol. I, 2nd ed. Malabar, FL: Krieger Publishing Company, 1990.

[25] G. Kovacs, M. Anhorn, H. E. Engan, G. Visintini, and C. C. W. Ruppel, "Improved material constants for $LiNbO_3$ and $LiTaO_3$," in *Proc. IEEE Ultrason. Symp.*, 1990, pp. 435–438.

[26] J. A. King, *Material Handbook for Hybrid Microelectronics.* Los Angeles, CA: Artech House, 1988, pp. 451–490.

[27] K. Yamanouchi and S. Hayama, "SAW properties of $SiO_2/128°$ Y–X $LiNbO_3$ structure fabricated by magnetron sputtering technique," *IEEE Trans. Sonics Ultrason.*, vol. SU-31, pp. 51–57, Jan. 1984.

[28] J. H. Hines, D. C. Malocha, K. B. Sudaram, K. J. Casey, and K. R. Lee, "Deposition parameter studies and surface acoustic wave characterization of PECVD silicon nitride films on lithium niobate," *IEEE Trans. Ultrason., Ferroelect., Freq. Contr.*, vol. 42, pp. 387–403, May 1995.

[29] E. G. Lean and C. G. Powell, "Optical probing of surface acoustic waves," *Proc. IEEE*, vol. 58, pp. 1939–1947, Dec. 1970.

[30] U. Rust, "Modellierung Integriert Akustooptisher Bauelemente in Lithiumniobat," Ph.D. dissertation, University of Paderborn, Paderborn, Germany, 1999. (in German)

[31] J. Frangen, H. Herrmann, R. Ricken, H. Seibert, W. Sohler, and E. Strake, "Integrated optical, acoustically tunable wavelength filter," *Electron. Lett.*, vol. 25, no. 23, pp. 1583–1584, Nov. 1989.

[32] D. A. Smith and J. J. Johnson, "Low drive-power integrated acoustooptical filter on X-cut, Y-propagating $LiNbO_3$," *Photonics Tech. Lett.*, vol. 3, pp. 923–925, Oct. 1991.

Oscar Antonio Peverini was born in Lisbon, Portugal, in 1972. He received the Laurea degree (summa cum laudae) in telecommunications engineering and the Ph.D. degree in electronic engineering at the Politecnico di Torino, Torino, Italy, in 1997, and 2001, respectively.

From August 1999 to March 2000 he was a visiting member at the Applied Physics/Integrated Optics Department of the University of Paderborn, Paderborn, Germany. In February 2001 he joined the Istituto di Ricerca sull'Ingegneria delle Telecomunicazioni e dell'Informazione (IRITI), an institute of the Italian National Research Council, Turin, Italy, (CNR) and since December 2001 he has been a Researcher of the IEIIT (Istituto di Elettronica e di Ingegneria dell'Informazione e delle Telecomunicazioni) a newly established institute of CNR. He teaches courses on electromagnetic field theory and applied mathematics at the Politecnico di Torino.

His research interests include numerical simulation and design of SAW waveguides and interdigital transducers for integrated acousto-optical devices, of microwave passive components and radiometers for astrophysical observations and microwave measurement techniques.

Harald Herrmann (M'97) received the diploma degree in physics (Dipl.-Phys.) from the University of Hannover, Hannover, Germany, in 1984. The same year he joined the Applied Physics/Integrated Optics group of the Physics Department of the University of Paderborn, Paderborn, Germany. There he is engaged in the development of integrated optical devices in $LiNbO_3$. In 1991 he received the Ph.D. degree in physics (Dr. rer. nat.) with a thesis on nonlinear frequency generation in optical waveguides.

In recent years his main interests are concentrated on the development of integrated acoustooptical and electrooptical devices in lithium niobate and their applications in optical communication systems and optical instrumentation.

Dr. Herrmann is a member of the IEEE and of the German Physical Society.

Renato Orga (M'93–SM'99) received the Laurea degree in electronic engineering in 1974 from the Politecnico di Torino, Torino, Italy. Since 1974 he has been a member of the Department of Electronics, Politecnico di Torino, first as an assistant professor, then as an associate professor and, since 1999, as a full professor.

In 1985 he was a Research Fellow at the European Space Research and Technology Center (ESTEC-ESA) at Noordwijk, The Netherlands. In 1998 he was a visiting professor (CLUSTER chair) at the Technical University of Eindhoven, The Netherlands. He currently teaches courses on electromagnetic field theory and on optical components.

His research interests include the areas of microwave and optical components, radiation and scattering of electromagnetic and elastic waves, and numerical techniques.